Investigating the Mechanism of Irreversible Failure in Pt/HfO$_2$/Ta/Pt Memristors

Nishat Tasnim Hiramony, Shafayeth Jamil, Zhiyuan Zhao, Ting-Hao Hsu, Himaddri Roy, Tanshia Tahreen Tanisha, and Wei Wu†

Viterbi School of Engineering, University of Southern California, Los Angeles, California 90089, United States, †wu.w@usc.edu

Memristors are promising building blocks for neuromorphic hardware because they combine non-volatility, low-energy operation, and multi-level conductance, suitable for analog weight storage. A persistent obstacle to reliable deployment is abrupt, irreversible failure - most commonly a transition to an "unresettable" state in which a once-switchable element becomes a permanent, metallic short due to runaway filament growth. Such hard failures can be triggered by voltage stresses, including electrostatic discharge, cumulative electrical stress, or operation beyond the safe compliance-current regime. Here, we investigate the physical origin of this failure mode by intentionally overstressing a Pt/HfO$_2$/Ta/Pt memristor stack with compliance currents exceeding the device's safe operating limit. This study will provide insight into enabling reliability-driven optimization of device stacks and programming conditions to mitigate sudden, unresettable breakdowns.

In these devices, the SET process is governed by field-driven migration of Ta species that forms a Ta-rich conductive filament through the HfO$_2$ switching layer. Under normal operation (≤ 2 mA compliance), switching remains reversible (Fig. 1a-d). When the compliance current exceeds ~2 mA, however, devices undergo a catastrophic transition to a stuck-ON low-resistance state with a complete loss of recoverable hysteresis (Fig. 1e-f). To elucidate the mechanisms underlying this irreversible transition, we employ a correlative workflow that combines electrical characterization (Fig. 1g) with nanoscale structural and compositional analysis. Post-failure AFM (Fig. 1h) reveals a distinct morphological fingerprint of hard breakdown: localized surface swelling with ~10 nm height increase and the emergence of Pt-rich mounds at the defect site. Notably, deprocessing by Ar ion milling indicates that these mounds are unusually resistant to sputter removal, consistent with recast and densified metallic material. Complementary SEM and EDS mapping (Fig. 1i-j) further confirm a pronounced enrichment of Pt at the defect site.

These observations support the occurrence of filament runaway under over-compliance stress. Excess current drives extreme current density within the conductive path, promoting lateral filament expansion and densification until the constricted "neck" region in the filament vanishes. Simultaneously, the large Joule heating and steep thermal gradients at the filament–electrode junction activate Pt mass transport through electromigration and thermomigration, leading to local electrode softening, extrusion, and accumulation directly above the hotspot. The resulting electric-field dilution due to thick filament reduces the local field during RESET to a level insufficient to reverse Ta transport and rupture the filament, locking the device into a permanent low-resistance state. We have combined kinetic Monte Carlo (kMC) modeling to capture Joule heating, filament thickening, and the resulting electric-field dilution that suppresses reset efficacy as the conductive path expands. In parallel, site-specific TEMs at the defect location have been done to resolve the cross-sectional morphology and composition of the dead filament and adjacent electrodes, providing a direct structural validation of the proposed failure mechanism. Details of these experimental results will be presented in the conference.

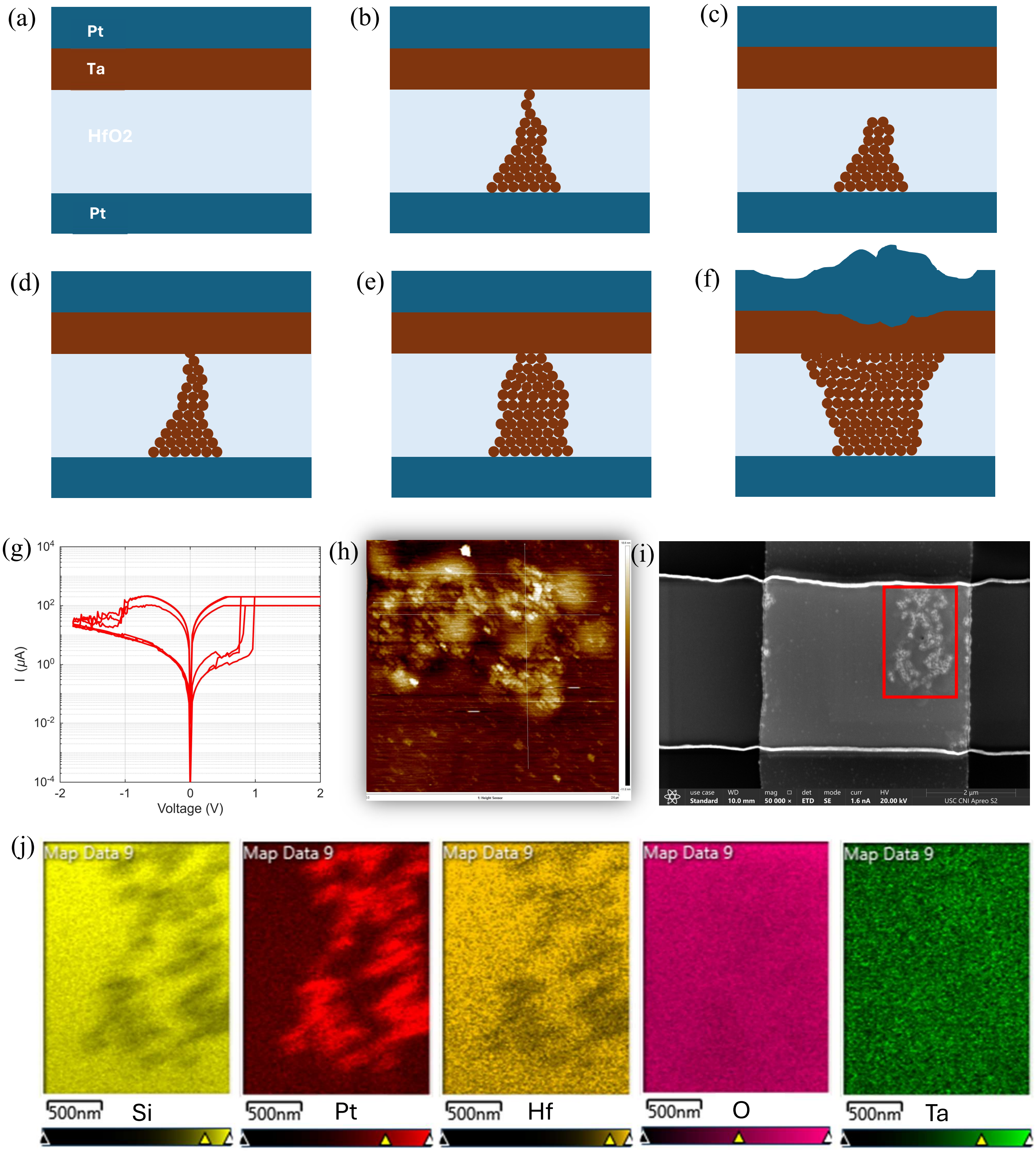

Fig. 1: Schematic illustration of (a) pristine device, (b) filament formation (forming), (c) RESET-induced rupture, (d) reversible SET with a narrow neck near the top electrode, (e) filament thickening with higher compliance current, and (f) runaway failure: permanent metallic plug formation with Pt hillock growth above the hotspot. (g) Representative I–V switching cycles with varying compliance current, (h) AFM topography of the failed region revealing localized surface swelling in top Pt (i) Top-view SEM image of the device; the red box marks the defect area selected for compositional mapping. (j) EDS maps (Si Kα1, Pt Mα1, Hf Mα1, O Kα1, Ta Lα1), showing a pronounced Pt-rich contrast spatially correlated with the damaged site.